SCIENCE CHINA
Information Sciences

• **RIVIEW** •

Key Issues and Algorithms of Multiple-Input-Multiple-Output Over-the-Air Testing in the Multi-Probe Anechoic Chamber Setup

Huiling PEI[1], Xiaoming CHEN[1*], Xiaobo LIU[1], Xiaotong ZHANG[2,3] & Yi HUANG[4]

[1]*School of Information and Communications Engineering, Xi'an Jiaotong University, Xi'an* 710049*, China;*
[2]*College of Electrical Engineering, Zhejiang University, Hangzhou* 310000*, China;*
[3]*Interdisciplinary Institute of Neuroscience and Technology, Zhejiang University, Hangzhou* 310000*, China;*
[4]*Department of Electrical Engineering and Electronics, University of Liverpool, Liverpool* L69 3GJ*, UK*

Abstract Multiple-input-multiple-output (MIMO) over-the-air (OTA) testing plays a key role in the research and development of wireless devices. MIMO OTA testing is necessary for fifth generation wireless products, in which conventional radio frequency ports are inaccessible. The performance of the test device can be evaluated in a repeatable and reliable way in laboratory conditions in OTA test, which might not be achievable in conducted test. Many efforts have been devoted to OTA test research and some achievements have been made. This paper mainly summarizes the channel emulation algorithms for two-dimensional user equipment and three-dimensional base station OTA testing in the anechoic chamber setup. In addition, the requirements of the test system design are also analyzed in this paper, including the selection of the number of OTA probes, the size of the test zone, the physical dimension of the setup, and the flexible probe selection algorithm of the three-dimensional base station OTA setup. In addition, some novel test methods for 5G radio devices are also discussed.

Keywords MIMO OTA testing, multi-probe anechoic chamber

Citation Pei H L, Chen X M, Liu X B, et al. Key Issues and Algorithms of Multiple-Input-Multiple-Output Over-the-Air Testing in the Multi-Probe Anechoic Chamber Setup. Sci China Inf Sci, for review

1 Introduction

Multiple-input-mutiple-output (MIMO) technology increases the channel capacity of the system without adding additional spectrum resources and antenna transmit power by installing multiple transmit and receiving antennas at the transmitter and receiver sides, respectively. New wireless technologies such as long-term evolution (LTE), LTE advanced, 802.11 and 5G have already adopted MIMO technology. Massive MIMO technology is widely used in 5G millimeter wave (mmWave) communication systems, which is due to the mmWave bands have a lot of available spectrum resources. However, high frequency propagation will cause the path loss to increase dramatically in the mmWave system. In order to compensate for the inherent loss of high frequency and achieve high signal power, mmWave systems need to install high-gain antennas. Fortunately, the increase of frequency means that the size of the antenna is reduced, so that the same space can accommodate more antennas, which facilitates the implementation of massive MIMO. To bring the massive MIMO technology from theory to practice, both academia and industry have invested tremendous efforts.

It is important for network operators to know the radio performance of MIMO devices before massive rollout in the network. Because over-the-air (OTA) testing [1, 2] was used to evaluate single-input-single-output performance, it is a suitable choice to assess the performance of MIMO systems. MIMO OTA testing is capable of reproducing radio propagation environment and thus can compare the different antenna configurations in the same environment [3].

* Corresponding author (email: xiaoming.chen@mail.xjtu.edu.cn)

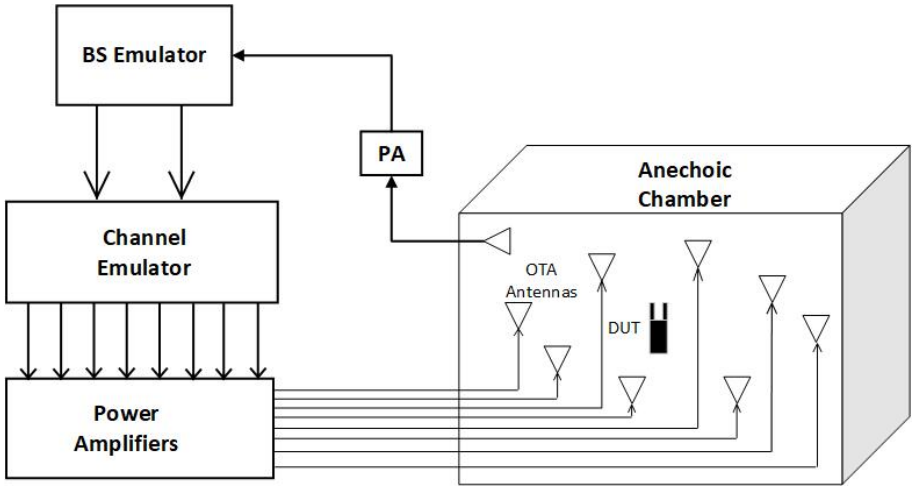

Figure 1 Illustration of the two-dimensional user equipment multiple-input-multiple-output over-the-air setup.

Many OTA test methods have been proposed. These methods differ in how to emulate the propagation channel, system size, and cost [4–7]. There are three categories of test methods: reverberation chamber-based methods [8, 9], radiated two-stage (RTS) methods [10, 11], and anechoic chamber-based methods [12–14]. The RTS method evolves from the conductive two-stage method [5] in which the cable connection between the channel emulator ports and the device under test (DUT) antenna ports is approached over-the-air. The multi-probe anechoic chamber (MPAC) setup is capable of reproducing any realistic and accurate radio propagation channel, and all critical parts are evaluated at once [15], making MPAC the most promising setup for MIMO OTA testing [16].

The main idea of channel emulation is to ensure the correct control of the signal is emitted from the probe antennas so that the emulated channel experienced by DUT approximates the target channel. The two common channel emulation methods are pre-fading signal synthesis (PFS) [6] and plane wave synthesis (PWS). PFS technology assigns appropriate power weights to probes to reproduce the spatial characteristics of the target channel at the receiver side [6, 17–19], whereas PWS technology assigns a suitable complex amplitude weight to each probe to reproduce the plane wave field of the target channel over the test zone. Additionally, a third method called equivalent induced voltage (EIV) is also proposed in this paper, which is implemented based on the similarity of the received voltage. In fact, the EIV method is also related to the field synthesis technique, because the received voltage is a response of antenna to the electric field in the test zone.

There are two popular MIMO channel models, geometric-based random channel models and correlation matrix based models. TGn model [20] is a typical correlation matrix based model. Geometric-based random channel models are usually selected to be the target channel model such as spatial channel model (SCM) and its extension (SCME), [21], WINNER [22] and 3GPP TR 38.901 [23]. Geometry-based modeling separates the antenna from the propagation, and the geometry and field pattern of the antenna can be defined independently of the propagation parameters.

The concept of clusters is widely used when simulating the multipath environment. A cluster has specific parameters including power angular spectrum (PAS) shape, angle of arrival (AoA), angle of departure (AoD), angle spread (AS), delay and power. Different clusters have different delays, making the channel wideband and PAS shape depends on the distribution of scattering components. User phantom has also been considered to achieve more reliable MIMO device performance evaluation [24, 25].

For standardized two-dimensional (2D) user equipment (UE) MIMO OTA testing, the DUT is in the center of the test zone, and probes are evenly distributed on a circular ring around the DUT (Figure 1). The DUT is placed on a polystyrene pedestal, which supports rotation and linear motion [26]. The base station (BS) simulator is used to create the original test signals. The channel simulator is used to connect to probes to create different spatial channels [27] and can create multipath environments including path delays, Doppler spread and fast fading. The power amplifiers adjust the signal to the desired power level [16]. The DUT is generally assumed in the far field of the OTA antennas.

Conventional BS antennas are tested by conducted methods, i.e., by connecting coaxial cables to the BS antenna ports. But for massive MIMO arrays, conducted test will require hundreds of cable

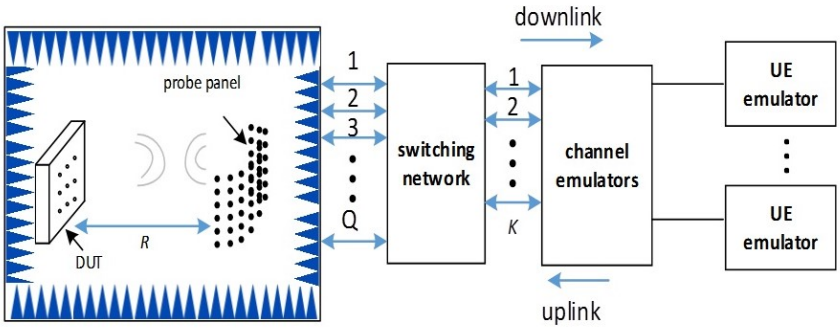

Figure 2 Illustration of the three-dimensional massive multiple-input-multiple-output base station over-the-air setup.

connections and corresponding hardware resources, which is very complicated and cost-prohibitive. A 3D cost-effective test setup called three-dimensional (3D) sectored MPAC setup is proposed for massive MIMO BS antennas OTA testing (Figure 2). This setup includes an anechoic chamber, a large number of OTA probes covering the angle area of interest, a controller used to select the active OTA antennas from the available OTA antennas, a switching circuit used to connect the active OTA antennas to the radio frequency (RF) interface ports of the channel emulator (CE), a CE, a DUT and a UE simulator (or multiple UEs) to mimic UE behavior [28]. The detailed reason for choosing this test setup will be given in Section IV.

The purpose of this review was to summarize the key algorithms and issues of MIMO OTA testing in the MPAC setup.

2 Testing of two-dimensional user equipment

The channel propagation environment is 3D in realistic physical world. 3D UE OTA testing has been studied in many literatures, which place multiple probe rings with different elevation angles. The channel emulation technique for arbitrary 3D channel models has been described [29, 30], and the first and last probe rings should be placed symmetrically to produce better emulation accuracy [31].

The PWS technique has been shown to be more accurate than PFS for most channel settings [32]. A group of radius of sphere and probe ring angular can achieve test performance for a fixed test zone when the target channel model is determined [33]. Typically, literature has described the test volume as sphere shaped, but the ellipsoid-shaped test volume has proven to be larger [34]. Since we have more probes placed in the azimuth plane than in the elevation plane, the ellipsoid-shaped test zone is selected. The probe selection method has been proposed for 3D MPAC setup [35] to limit cost, and use of the method has revealed that the multi-shot algorithm produces the best accuracy.

However, some proposed algorithms [35] do not minimize the number of selected probe sets. To address this, one study [36] described the decremental selection algorithm (DSA) and the error threshold selection algorithm based on alternating search (SAAS). These algorithms minimize the number of probes while ensuring the accuracy of the target channel emulation. Notably, SAAS provides better performance than DSA. To further improve simulation accuracy and reduce related costs, a flexible multi-probe setup for 3D emulation has been proposed in which the probe is mounted on a movable semi-arc track for flexible probe placement at both elevation and azimuth angles. Two probe selection algorithms, the genetic and multi-shot algorithms, have been proposed to verify the feasibility and accuracy of this setup [37].

A 3D flexible MPAC setup has been shown [38] to perform better compared with a fixed setup in terms of spatial correlation emulation. Another original channel emulation method, called the reference method for 3D channel [39], focused on using a simple technique to allocate subpaths (i.e. the combination of uniform angle and power sampling). This method is more accurate than the spatial fading emulator method under the same conditions and addresses the shortcomings of the PFS method.

But in fact, most of the standardized radio channel models such as WINNER and CSM channel model, are 2D in the sense that they use only geometrical xy-coordinates (azimuth plane). Elevation dimension has been left out due to considerably smaller angular spread in elevation dimension than in azimuth [6].

This section mainly summarizes channel emulation methods for 2D UE MIMO OTA testing. Metrics to evaluate the accuracy of channel emulation are also discussed. In addition, requirments for 2D MPAC

setup design are also contained in this section. Typical channel emulation methods include PFS and PWS, but another technique called EIV (which focuses on reproducing target received voltage) is also described in this section. This paper does not cover the direct sampling technique because it is less accurate compared with the methods using optimized weights for the PFS technique [40–42].

Several studies [43, 44] have concluded that three factors result in measurement inaccuracies: pedestal instability after sledge movement, field variation over rotation at test area center and reflections. The sources of inaccuracies are DUT placement error, cable effect and reflections inside the chamber. For example, cable effect will distort the radiation pattern of the DUT and hence affect the measurements [43].

Before the OTA testing, the channel model needs to be verified at the DUT location [45] to ensure that the DUT can be tested in the desired channel environment. The verification process involves some important parameters, including power delay distribution, temporal correlation, spatial correlation and cross-polarization power ratio. The specific verification process has been described [46].

It is important to calibrate the OTA system before taking measurements. The main purpose of the calibration is to eliminate non-idealities of the system such as the impact of probe placement errors on the measurement [47]. In one study [47], performance deterioration introduced by system non-idealities was investigated in terms of spatial characteristics, whereas another [48]investigated performance deterioration introduced by system non-idealities in terms of field synthesis.

2.1 Channel emulation algorithm

2.1.1 *Pre-fading signal synthesis method*

The idea of the PFS method is to transmit power-weighted Rayleigh or any other fading signals from multiple independent probes to reproduce the spatial characteristics of the target channel measured at the receiver side. Spatial correlation has been selected as the metric to characterize the spatial characteristics at the Rx side. To reconstruct the PAS of the target channel, suitable probe power weights are generated for each cluster. The antenna correlation in the target channel can be written as

$$\rho = \frac{\int_{-\pi}^{\pi} G_{q1}(\phi) G_{q2}^{*}(\phi) P(\phi) d\phi}{\sqrt{\int_{-\pi}^{\pi} P(\phi) |G_{q1}(\phi)|^2 d\phi} \sqrt{\int_{-\pi}^{\pi} P(\phi) |G_{q2}(\phi)|^2 d\phi}}. \tag{1}$$

where $G_{q1}(\phi)$ and $G_{q2}(\phi)$ are complex radiation patterns of antenna pair (q_1, q_2); ϕ represents the AoA of the incoming wave; $P(\phi)$ represents the continuous power angle spectrum of the target channel.

Since the antenna pattern of the DUT is included already in the measurement system, it is assumed that the DUT is omnidirectional. The spatial correlation of the target channel can be written as

$$\rho(q_1, q_2) = \int_{-\pi}^{\pi} \exp\left(j2\pi/\lambda \left(\vec{p}_{q1} - \vec{p}_{q2}\right) \cdot \phi\right) P(\phi) d\phi, \tag{2}$$

where λ is wavelength; $\vec{p}_{q1}$ and $\vec{p}_{q2}$ are position vectors of the antenna pair (q_1, q_2).

Assuming that the wave received by the DUT in the test area is an ideal plane wave, the spatial correlation of the emulated channel can be written as

$$\hat{\rho}_{ideal} = \sum_{k=1}^{K} g_k \exp\left(j2\pi/\lambda \left(\vec{p}_{q1} - \vec{p}_{q2}\right) \cdot \bar{\phi}_k\right), \tag{3}$$

where g_k represents the power weight of the kth probe; K is the number of the probes; $\bar{\phi}_k$ is the unit position vector of the kth probe.

Let $\boldsymbol{\rho}$ and $\hat{\boldsymbol{\rho}}_{ideal}$ represent the target channel spatial correlation vector and the emulated channel spatial correlation vector under the ideal plane wave assumption, respectively. The objective function is based on the above two sets of spatial correlation.

$$min \parallel \hat{\boldsymbol{\rho}}_{ideal}(\boldsymbol{g}) - \boldsymbol{\rho} \parallel_2^2 . \tag{4}$$

The spatial correlation is selected as the objective function without constraints on the PAS shape [6, 18,19,49]. However, owing to the limited number of the test samples, different shapes of PASs may result in similar spatial correlation. Therefore, a limitation on the shape (average AoA and AS) of the PAS is introduced; that is, the PAS of the target channel is accurately simulated by limiting the deviation

between the simulated average AoA and AS and the target average AoA and AS [50]. The above quadratic programming problem with linear constraints can be easily solved by convex optimization [51]. Note that if a small anechoic chamber is used to reduce cost, the emulated spatial correlation will introduce the spherical wave effect, and the emulated spatial correlation can be written as

$$\hat{\rho}_{small} = \frac{\sum_{k=1}^{K} g_k \cdot F_{k,u} F_{k,v} \exp\left(j2\pi\left(d_{k,u} - d_{k,v}\right)/\lambda\right)}{\sqrt{\sum_{k=1}^{K} F_{k,u}^2 g_k \sum_{k=1}^{K} F_{k,v}^2 g_k}}, \tag{5}$$

where $F_{k,u}$ and $F_{k,v}$ are path loss terms from the kth probe to uth and vth DUT elements, respectively; $d_{k,u}$ and $d_{k,v}$ are distances from the kth probe to uth and vth DUT elements, respectively. In this case, the field within the test area includes both the desired signals from the probes and the undesired signals caused by reflections and coupling among the probes. Therefore, the chamber compensation technique can be used to reduce undesired paths [52, 53].

If the DUT antenna pattern is considered, the emulated antenna correlation in the OTA case can be written as

$$\hat{\rho} = \frac{\sum_{k=1}^{K} G_{q1}\left(\phi_k\right) G_{q2}\left(\phi_k\right) g_k}{\sqrt{\sum_{k=1}^{K} |G_{q1}\left(\phi_k\right)|^2} \sqrt{\sum_{k=1}^{K} |G_{q2}\left(\phi_k\right)|^2}}. \tag{6}$$

The number of probe antennas that can achieve sufficient correlation accuracy for ideal DUTs may not achieve sufficient accuracy for realistic DUTs when the antenna pattern varies fast [54]. Therefore, DUT patterns should be considered to determine the number of probes. But for realistic DUT at sub 6GHz, the DUT antenna pattern is quasi-omnidirectional. Therefore, we often do not consider the antenna pattern when we need to determine the number of required probes.

Once the power weights of the probes are determined, the channel coefficients simulated by the PFS method are also determined. Note that the channel coefficients ignore the patterns of the probe antennas and the path loss of free space. There are U receiving antennas and S transmitting antennas, and for simplicity only vertical polarization is considered.

$$\begin{aligned} \hat{h}_{u,s,n}^{PFS}(t,f) = & \sqrt{\frac{P_n}{M}} \sum_{k=1}^{K} \sum_{m=1}^{M} F_s^{\mathrm{Tx}}\left(\varphi_{n,m}\right) F_u^{\mathrm{Rx}}\left(\phi_k^{OTA}\right) \\ & \cdot \sqrt{g_{n,k}} \cdot \exp\left(j2\pi v_{n,m} t + j\Phi_{n,m,k}\right) \cdot \exp\left(-j2\pi f \tau_n\right), \end{aligned} \tag{7}$$

where P_n is the power of the nth cluster; M is the number of subpaths in each cluster; F_s^{Tx} and F_u^{Rx} are the field pattern of sth Tx antenna and uth Rx antenna, respectively. Note that the field pattern is defined with a common phase center. $v_{n,m}$ is the Doppler frequency of the mth subpath of the nth cluster; τ_n is delay of the nth cluster; $\Phi_{n,m,k}$ s the random initial phase generated for each subpath of each cluster. Note that for each probe, the random initial phase is independently generated.

2.1.2 *Plane wave synthesis method*

The target field is approximated by superposing the fields from probes for the PWS method. Note that the probe weights are generated for each subpath instead of for each cluster. The generation of plane waves relies on assigning appropriate complex weights to different probes. The PWS technique can be implemented based on plane waves [6, 55] or by using a spherical wave theory to synthesize desired electromagnetic field environment [12,56]. Although the PWS method is traditionally based on the plane waves, the spherical wave theory is preferred because it includes near-field effects during the synthesis of electromagnetic environments [14].

Only the vertical polarization is considered for simplicity. For a single plane wave, according to the least squares technique [57], the optimization problem can be solved with the following equation

$$\mathbf{FW} = \mathbf{T}, \tag{8}$$

where $\mathbf{T}$ is the target field; $\mathbf{F}$ is the coefficient transfer matrix from the probes to the sampling points over the test area; $\mathbf{W}$ is the weight vector to be solved. Assuming that the M-point sampling is performed in the test area and M is greater than K (the number of probes), then the optimization problem becomes

an over-determined problem, and the weight vector can be obtained by solving the following problem of minimizing the 2-norm

$$\min_{\mathbf{w}} \parallel \mathbf{FW} - \mathbf{T} \parallel . \tag{9}$$

From this, we can get

$$\mathbf{W} = \left(\mathbf{F}^H\mathbf{F}\right)^{-1}\mathbf{T}^H\mathbf{T}. \tag{10}$$

For vertical polarization, both the target field and the emulated field are perpendicular to the xy plane. For horizontal polarization, the target field is on the xy plane and perpendicular to the AoA, whereas the emulated field is on the xy plane and perpendicular to the AoA where the probe is located. To accurately emulate the horizontal polarization field, the optimization must be decomposed to two orthogonal axes x and y as

$$\min_{\mathbf{w}} \left\| \begin{bmatrix} \mathbf{F}_x \\ \mathbf{F}_y \end{bmatrix} \mathbf{W} - \begin{bmatrix} \mathbf{T}_x \\ \mathbf{T}_y \end{bmatrix} \right\|_2^2 \tag{11}$$

and it can be easily solved by convex optimization. The correlation accuracy is the same for large R [54].

Using spherical wave extension, the electric field of a time-harmonic plane wave from the free space can be expressed as

$$\vec{E}\left(r,\theta,\phi\right) = \frac{k}{\sqrt{\eta}} \sum_{s=1}^{2} \sum_{n=1}^{\infty} \sum_{m=-n}^{n} Q_{smn}^{(1)} \vec{F}_{smn}^{(1)}\left(r,\theta,\phi\right), \tag{12}$$

where k is the wave number; η is the admittance of the medium; s, m, n represents the mode index of the spherical wave; $Q_{smn}^{(1)}$ is a spherical wave coefficient for a spherical standing wave; $\vec{F}_{smn}^{(1)}$ is the corresponding spherical vector wave function in the standard spherical coordinates. Due to the cut-off property of the spherical wave function [58], especially that of the spherical Bessel function and its derivative function, (12) can be written as

$$\vec{E}\left(r,\theta,\phi\right) = \frac{k}{\sqrt{\eta}} \sum_{s=1}^{2} \sum_{n=1}^{N} \sum_{m=-n}^{n} Q_{smn}^{(1)} \vec{F}_{smn}^{(1)}\left(r,\theta,\phi\right), \tag{13}$$

where N is the truncation number, $N = \lceil kr_0 + n_1 \rceil$. r_0 is the radius of the test area; n_1 is a small integer used to control the accuracy of the emulation. $\lceil \cdot \rceil$ denotes round up operation. Similarly, the radiated field of a probe can be written as

$$\vec{E}_k\left(r,\theta,\phi\right) = \frac{k}{\sqrt{\eta}} \sum_{j=1}^{J} w_k P_j^k F_j^{(1)}\left(r,\theta,\phi\right), \tag{14}$$

where w_k s the voltage of the kth probe; J is the number of spherical wave modes; P_j^k is a spherical wave coefficient of probe radiation patterns. To reproduce the target field in (13), we can obtain an equation

$$\begin{bmatrix} P_1^1 & P_1^2 & \cdots & P_1^K \\ P_2^1 & P_2^2 & \cdots & P_2^K \\ \vdots & \vdots & \ddots & \vdots \\ P_J^1 & P_J^2 & \cdots & P_J^K \end{bmatrix} \begin{bmatrix} w_1 \\ w_2 \\ \vdots \\ w_k \end{bmatrix} = \begin{bmatrix} Q_1 \\ Q_2 \\ \vdots \\ Q_J \end{bmatrix}. \tag{15}$$

This equation can be written as a matrix form like $\mathbf{PQ} = \mathbf{W}$. Then the probe voltage vector can be obtained by the Moore-Penrose pesudo-inverse as

$$\mathbf{W} = \mathbf{P}^{+}\mathbf{Q} = \left(\mathbf{P}^H\mathbf{P}\right)^{-1}\mathbf{P}^H\mathbf{Q}. \tag{16}$$

If the Doppler shift is introduced to the system to consider a time-varying channel, the time-varying weight is obtained by multiplying the complex weight by the rotation phasor.

$$w_k\left(t\right) = w_k \exp\left(-jtw_d\right), \tag{17}$$

where w_d is the Doppler shift, which can be determined by the wave vector $\vec{\beta}$ and the moving speed $\vec{v}$ of the DUT.

$$w_d = -\vec{\beta} \cdot \vec{v} \tag{18}$$

Another method to consider the time-varying channel is that each snapshot is considered static [12]. It outperforms because arbitrary multipath environments can be reduced.

Once the complex amplitude weights of the probes are determined, the channel coefficients emulated by the PWS method are also determined. Note that the channel coefficients also ignore the patterns of the probe antennas and the path loss of free space. Again, only vertical polarization is considered for simplicity.

$$\begin{aligned} \hat{h}_{u,s,n}^{PWS}(t,f) = & \sqrt{\frac{P_n}{M}} \sum_{m=1}^{M} \sum_{k=1}^{K} F_s^{\mathrm{Tx}}(\varphi_{n,m}) F_u^{\mathrm{Rx}}\left(\phi_k^{OTA}\right) \\ & \cdot w_{n,m,k} \cdot \exp\left(j2\pi v_{n,m} t + j\Phi_{n,m}\right) \cdot \exp\left(-j2\pi f \tau_n\right), \end{aligned} \tag{19}$$

where $w_{n,m,k}$ is the complex weight of the kth probe of the mth subpath of the nth cluster.

If the modeling of the Ricean channel is involved, the line of sight (LOS) path can be emulated by the PWS method, whereas the other non-LOS clusters are simulated by the PFS method [58]. At this time, it should be noted that for the LOS path, power and phase calibration are both required, but only power calibration is required for other paths.

The space-time correlation analysis has been performed for the above two emulation methods [59], which revealed that the power AoA-AoD spetrum has a Kronecker structure in the PFS method.

2.1.3 *Equivalent induced voltage technique*

The goals of PFS and PWS methods are to reproduce the correlation at the Rx side and to reconstruct the target field within the test area, respectively. In contrast, the EIV method aims to reproduce the target received voltage by assigning appropriate complex weight to each probe.

The received voltage is not only determined by the impinging plane waves but by antenna patterns. The target received voltage can be defined as

$$V = E_0 \cdot L(\phi), \tag{20}$$

where E_0 is the electric density of incident field and L is the antenna radiation pattern. The emulated received voltage in the OTA case can be defined as

$$\hat{V} = \sum_{k=1}^{K} V_k = E_0 \cdot \sum_{k=1}^{K} g_k(\phi) L(\phi_k) = E_0 \cdot \hat{L}(\phi), \tag{21}$$

where $\hat{L}(\phi)$ is the emulated antenna radiation pattern at plane wave arrival direction ϕ. Our goal was to optimize g_k to ensure that V is equal to $\hat{V}$. The $g_k(\phi)$ can be obtained by using trigonometric interpolation [60] as

$$g_k(\phi) = \frac{1}{K} \sum_{k=1}^{K} \cos m(\phi - \phi_k), \tag{22}$$

where $m = k - \lceil K/2 \rceil$. Then we can solve for the complex weight assuming that the phase at the test zone center is 0 as

$$g_k^{\mathrm{TI}}(\phi) = g_k(\phi) \exp(-j\beta R), \tag{23}$$

where β is the wave number. The EIV method generates the same complex weights as the PWS method when R is large [54].

2.2 Channel emulation accuracy

There are some metrics to evaluate how well the emulated channel approximates the target channel, including spatial correlation error, field synthesis error, capacity error, throughput error and PAS error.

2.2.1 *Spatial correlation error*

In order to evaluate the difference between the target spatial correlation and the emulated spatial correlation, the spatial correlation error (i.e. $|\rho - \hat{\rho}|$) is selected as the figure of merit (FoM). When $|\rho|$ is high, spatial correlation error is more critical, which means the performance of MIMO system is sensitive to spatial correlation. On the contrary, spatial correlation error is less critical when $|\rho|$ is small [61].

2.2.2 *Field synthesis error*

In order to evaluate the error between the target field and the emulated field, the field synthesis (i.e. $\left|E - \hat{E}\right|$) is selected as the FoM, where E and $\hat{E}$ represent the target and emulated field, respectively [57].

2.2.3 *Capacity error*

MIMO channel matrix in frequency domain has been obtained in sections 2.1 and 2.2. We assume that channel state information is not available at the Tx side. Therefore, equal power is assumed among Tx antennas, and the channel capacity is calculated based on this assumption. The instantaneous channel capacity of the target channel can be written as [62]

$$C(t) = \frac{\sum_{n_f=1}^{N_f} \log_2 \det\left(\mathbf{I} + \frac{\sigma}{\eta \cdot S} \cdot \mathbf{H}(t, n_f) \cdot \mathbf{H}(t, n_f)^H\right)}{N_f}, \tag{24}$$

where N_f is the number of subcarriers; σ is signal to noise ratio; S is the number of Tx antennas; η is the power normalization factor to ensure the received power is 1. Note that N_f has to be large enough to ensure that each sub-channel experiences flat fading.

Let C and $\hat{C}$ represent target and emulated channel capacity, then the capacity error is $\left|C - \hat{C}\right|$. However, channel capacity only indicates the theoretical upper bound of the data rate, and cannot directly reflect practical MIMO terminal performance [63].

2.2.4 *Throughput error*

Throughput error is used to characterize the channel emulation accuracy in order to reflect the end-to-end performance of the system. Throughput error is the difference between the target and emulated throughput. The measurement method of system throughput will be described in 2.3.2.

2.2.5 *PAS error*

PAS is very important for the reconstruction of the channel in the spatial domain. As described in 2.1, different shapes of PASs may result in similar spatial correlation. Therefore, PAS error is a very important FoM to measure the accuracy of channel emulation. Methods to emulate the multi-cluster PAS are discussed in [49].

2.3 Rrequirements of the 2D UE test system design

2.3.1 *Number of over-the-air probes*

The number of required OTA antennas in MPAC setup has been studied in many literatures. Studies have shown that the number of OTA probes is related to DUT size, channel model, OTA probe locations, and acceptable error levels for FOMs discussed in 2.2. A rule of thumb of the number of OTA antennas is shown in [6]. General rules for the required number of probes have been proposed [64–68]. In theory, an infinite number of OTA antennas are required to synthesize any electromagnetic field over the test zone, which is unrealistic. From (13), we can solve for the number of spherical wave modes using $J = 2N(N+2) = 2\left(\lceil kr_0 + n_1 \rceil\right)^2 + 4\left(\lceil kr_0 + n_1 \rceil\right)$. To accurately generate these J modes, the minimum number of probes should be equal to J, i.e.

$$K_{MIN} = 2\left(\lceil kr_0 + n_1 \rceil\right)^2 + 4\left(\lceil kr_0 + n_1 \rceil\right). \tag{25}$$

Equation (25) considers the 3D case, but because the elevation angle range near the UE is typically narrow, the elevation angle is often assumed to be fixed at 90°. Then the 3D case is simplified to the 2D

Table 1 n_1 for different equivalent reflectivity level

Equivalent reflectivity level ε	n_1
-10dB	$0.37\times \sqrt[3]{kr_0}$
-15dB	$0.74\times \sqrt[3]{kr_0}$
-20dB	$1.08\times \sqrt[3]{kr_0}$
-25dB	$1.45\times \sqrt[3]{kr_0}$
-30dB	$1.85\times \sqrt[3]{kr_0}$

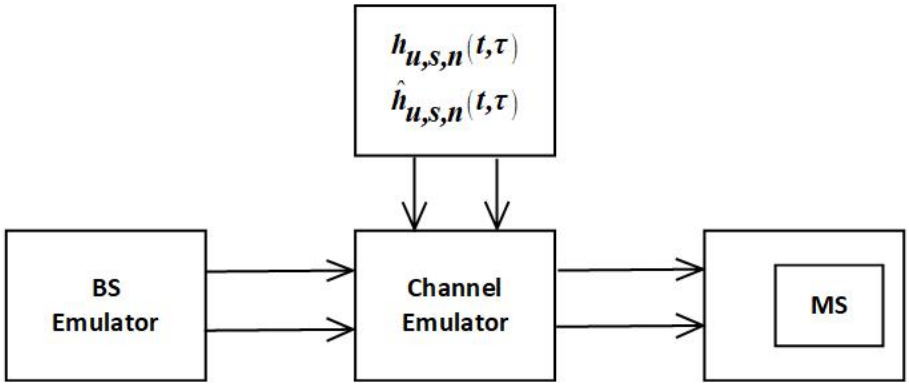

Figure 3 Synthetic multi-probe anechoic chamber setup.

case, with the mode number J changed to $J = K_{MIN}^{2D} = 2(2N+1) = 4(\lceil kr_0 + n1 \rceil) + 2$. To obtain a more accurate number of probes in the 2D case, the value of n_1 is crucial. The relation between n_1 and r_0 is $n_1 = o\left(\sqrt[3]{kr_0}\right)$ [69]. The values of n_1 are listed in Table 1 for different equivalent reflectivity level ε (the maximum relative error between the emulated field and target field) [70].

2.3.2 *Test zone size*

One of the key issues to address in the MPAC setup is how large of a test area can be supported. Test zone characterization [71] has been studied. Many metrics can be used to determine the test zone size, such as field synthesis error and spatial correlation error. It is difficult to define acceptable error thresholds for field synthesis error and spatial correlation error, as these error thresholds cannot be directly reflected in data rate deviation. Because the throughput can reflect the end-to-end performance of the test system, the throughput error is chosen as the metric to characterize the test zone size. However, in principle, an infinite number of OTA probes are required in the MPAC setup to reproduce the accurate target channel model as a reference for determining throughput error, which is not feasible. The synthetic MPAC setup (Figure 3) has been proposed to address this challenge [63, 72].

The channel matrix is embedded in the channel emulator in the synthetic MPAC setup, and then the throughput measurement is performed in the conductive manner. During the measurement process, different MPAC configurations and different antenna spacings can be flexibly changed because the MPAC configuration and antenna spacing can be arbitrarily set in equation (7).

The influence of user phantom on the test zone size has also been considered [72]. Placing a user phantom in the vicinity of the DUT has two major effects on MIMO performance.

1) detuning of the antennas by bulky dielectrics;

2) blocking and scattering of the incoming waves.

Similarly, the synthetic MPAC setup has also been used [72] for throughput measurement. At the same time, the emulation accuracy of other figure of metrics was also considered, including received power, branch power ratio, and antenna correlation. The results showed that the presence of user phantom near the DUT does not affect the simulation accuracy of metrics, so the impact of user phantom on the test zone size is negligible.

2.3.3 *Physical dimension of the setup*

The physical dimension of the setup is determined based on an acceptable error on amplitude distribution of spatio-temporal fading when the system considers field strength stability [73]. Other criteria such as

power imbalance and correlation error are more directly related to the spatial characteristics of channel models for determining physical dimensions.

1) Power imbalance

Considering one probe and free space loss, the Rx power ratio between two locations on the test area can be written as

$$\Delta P = \frac{L\left(d_1, \lambda\right)}{L\left(d_2, \lambda\right)} = \left(\frac{d_1}{d_2}\right)^2, \tag{26}$$

where d_1 and d_2 are the distances from the probe to the locations on the test area; L is free space loss, which is defined as

$$L\left(d, \lambda\right) = \left(\frac{4\pi d}{\lambda}\right)^2. \tag{27}$$

when the probe is on the same line with Rx antennas and the distance between two Rx antennas is $2r_0$, maximum power difference can be achieved as

$$\Delta P_{\max} = 10\log_{10}\left(\frac{1 + r_0/R}{1 - r_0/R}\right), \tag{28}$$

where R is the physical dimension of the test setup. The average imbalance can be defined as

$$\Delta P_{\text{aver}} = 10\log_{10}\langle d_{q1,k}^2 / d_{q2,k}^2 \rangle, \tag{29}$$

where q_1, q_2 denotes location pairs of the test area; $\langle\cdot\rangle$ denotes represents the average operation.

2) Correlation error

Correlation error is the deviation between the emulated correlation in ideal conditions and the emulated correlation in physically constrained setup, i.e.

$$E_\rho = \hat{\rho}_{ideal} - \hat{\rho}_{small}. \tag{30}$$

Note that the correlation error not only considers field strength stability, but also considers phase stability. If we have selected error thresholds, the physical dimension R can be determined as a function of r_0. One study [74] escribed the relationship between R and r_0 as $R = 0.1r_0$ if 0.05 rms of correlation error and 0.5dB of average power imbalance are selected as error thresholds.

To save laboratory space and reduce system costs, a small anechoic chamber may be applied; however, the waves illuminating the test area will have curved phase fronts. A plane wave compensation technique has been proposed in small MPAC setups to minimize spherical effects [75]. It can be seen from equation (5) that path loss and phase error have important effects on emulated spatial correlation in a small MPAC setup. The core of the proposed compensation technique is that a far-field probe is emulated by a few near-field probes, and they are connected to different programmable power attenuators and phase shifters but one output of the channel emulator (Figure 4). The flexible probe setup is used to improve the compensation accuracy, and the particle swarm optimization (PSO) algorithm is adopted to obtain far-field angle locations of probes.

Suppose there are K far-field probes, each of which uses $\hat{K}$ near-field probes to emulate. Then the channel frequency response (CFR) from sth Tx antenna to kth probe of nth cluster can be written as

$$h_{s,k,n}^{\text{OTA}}\left(t, f\right) = \sqrt{\frac{P_n}{M}} \sum_{\hat{k}=1}^{\hat{K}} \sum_{m=1}^{M} F_s^{\text{Tx}}\left(\varphi_{n,m}\right) g_{k,\hat{k},n} \cdot \exp\left(j2\pi v_{n,m} t + j\Phi_{n,m,k}\right) \cdot \exp\left(-j2\pi f \tau_n\right), \tag{31}$$

where $g_{k,\hat{k},n}$ denotes the complex weight of $\hat{k}$th near-field probe of kth far-field probe of nth cluster. It is demonstrated that this plane compensation technique improves the system performance in terms of field distribution, spatial correlation and PAS estimation. That is, conventional far-field criteria can be relieved to implement a small MPAC setup to save costs.

2.3.4 *State-of-art works*

There is still much work can be done to improve the 2D PMAC setup design, for example, the impact of different MS designs and channel models on the test zone size in terms of throughput deviation and the impact of correlation error and power imbalance on DUT performance indicators.

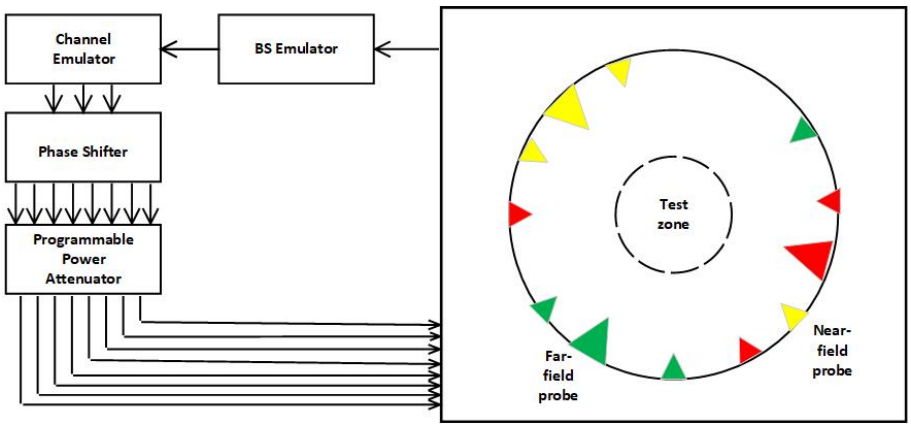

Figure 4 Multi-probe anechoic chamber setup involving the plane wave compensation technique.

3 Three-dimensional massive base station testing

Use of massive MIMO technology is a promising approach to achieving considerably improved spectral efficiency in 5G communication. Conducted testing is no longer suitable for 5G antenna systems for several reasons. First, 5G antennas are highly integrated units and the number of the antennas will be very large, resulting in unavailable antenna connectors owing to cost, size and design challenges. Second, 5G antenna systems equipped with possibly hundreds of antennas will need hundreds of RF cable connections and corresponding hardware resources, which is infeasible and costly. Finally, the features of 5G antenna systems rely heavily on their spatial discrimination capability, which cannot be evaluated in the conductive manner [76]. Therefore, MIMO OTA testing is required for 5G antenna systems.

The applicability of the three UE MIMO OTA test methods (i.e. RC, RTS, and MPAC) for massive MIMO BSs can be compared. The RC-based method does not provide angular distribution and cross-polarization discrimination of the channel. Because the millimeter-wave channel is highly sparse and directive, the RC-based method is not suitable for OTA testing of adaptive millimeter-wave antenna systems. Because the RTS method requires measurement of the antenna patterns in the first stage, it is not suitable for dynamic adaptive beamforming systems [77]. Additionally, in the RTS method, the number of OTA antennas should be equal to the number of DUT antennas, resulting in a large number of active OTA antennas, which is costly.

The MPAC-based method is attractive for massive MIMO BS OTA testing as it is capable of physically simulating the actually multipath environment in an anechoic chamber. The adaptive antenna technology can also be reliably emulated in the MPAC setup. A 3D sectored MPAC setup has been proposed for massive MIMO BS OTA testing [78]. The 3D sectored MPAC setup is more suitable for massive MIMO BS OTA testing for multiple reasons [79]:

1) The BS is placed higher and away from scatters, so the angular spread at the BS side is relatively small.

2) The coverage area of the BS antenna array is usually limited to a certain range of angles, such as 60^{o} or 120^{o}.

3) The sectored MPAC device can considerably reduce system cost by reducing the required fading emulators and corresponding hardware resources. Because the DUT is placed at one end of the anechoic chamber, the size of the entire chamber is used.

The hardware resources required by the sectored and uniform MPAC setups to achieve the same correlation error level have been compared [80] (Table 2). The sectored MPAC setup can noticeably reduce the system cost while ensuring the accuracy of the emulation.

This section mainly summarizes channel emulation methods for 3D BS MIMO OTA testing. In addition, a few new metrics are explained to evaluate the accuracy of channel emulation and some novel test methods are also been discussed.

To ensure that the target channel models are accurately emulated, validation of emulated channel models in the sectored MPAC setup is required. The joint angle-delay power profile is selected as the metric for the validation for 5G beamforming management performance evaluations. Two estimation

Table 2 sectored vs uniform multi-probe anechoic chamber hardware required to achieve desired correlation error level

channel model	SCME UMa	SCME UMi	SCME UMa	SCME UMi
rms e_ρ	0.1	0.05	0.26	0.09
sectored MPA	K=12 $116m^2$	K=16 $116m^2$	K=12 $29m^2$	K=16 $29m^2$
uniform MPAC	K=60 $400m^2$	K=100 $400m^2$	K=60 $100m^2$	K=100 $100m^2$

algorithms, the joint angle and delay estimation (JADE) and sequential search algorithm, are considered. It has been concluded [81] that both algorithms provide good estimation accuracy. Notably, the sequential search algorithm provides a little more accuracy and offers lower computation complexity because of the sequential estimation in different domains instead of joint estimation.

Some studies [82, 83] have noted that for massive MIMO and high-frequency scenario testing, the field synthesis method requires more probe antennas to achieve a sufficiently accurate emulation. Moreover, for the upcoming 5G communication system, phase calibration of the BS OTA testing is difficult owing to the non-linearity of the radio frequency components such as the switching network and power amplifiers. Therefore, use of the channel emulation method is limited to the PFS method.

3.1 Channel emulation algorithm

The idea of the PFS method is mainly to reproduce the spatial characteristics of the target channel at the Rx side by assigning appropriate power weights to the limited active probes in the MPAC setup. The following two methods optimize probe weights:

1) Similarity of the spatial correlation

First, the DUT needs to be mechanically rotated so that the clusters with higher powers and as many clusters as possible fall within the sector of interest of the BS. One study [28] proposed a rotation scheme based on the center gravity of the target PAS. However, this rotation scheme neglects the effects of weaker clusters, leading to simulation errors. A novel rotation scheme has been proposed [84] to maximize the total power of the clusters covered by the probe wall.

Next, select the appropriate probes through the switching network. According to the descending order of cluster powers, each cluster is allocated an active probe that is nearest to the cluster angle until K probes are allocated. If the number of clusters falling within the sector is less than K, then allocate as many probes as possible for the cluster with the highest power, and so on, until the K probes are allocated [28]. Another proposed probe allocation algorithm [84], the forward allocation (FA) algorithm, has shown better performance. For a pair of spatial locations $q = \left(\mathbf{p}_{q1}, \mathbf{p}_{q2}\right)$, the target spatial correlation is defined as

$$\rho_q = \oint P\left(\Omega\right) \exp\left(j\Omega \cdot \left(\mathbf{p}_{q1} - \mathbf{p}_{q2}\right)\right) d\Omega, \tag{32}$$

where Ω denotes the wave vector to the spatial angle Ω; $P\left(\Omega\right)$ is the continuous power angle spectrum of the target channel. Because the far-field requirement is usually not met in the massive MIMO BS OTA testing, the emulated spatial correlation in the OTA case must consider the gain and phase errors caused by the spherical waves [85]. The spatial correlation in the OTA case is defined as

$$\hat{\rho}_q = \frac{\sum_{k=1}^{K} g_k L\left(d_{p1,k}\right) L\left(d_{p2,k}\right) \exp\left(j \parallel \Omega \parallel \left(d_{p1,k} - d_{p2,k}\right)\right)}{\sqrt{\sum_{k=1}^{K} L^2\left(d_{p1,k}\right) g_k} \sqrt{\sum_{k=1}^{K} L^2\left(d_{p2,k}\right) g_k}}, \tag{33}$$

where g_k is the power weight of the kth active OTA probe and $\parallel \Omega \parallel = \dfrac{2\pi}{\lambda}$; $L\left(d_{p1,k}\right)$ and $L\left(d_{p2,k}\right)$ are the path loss terms of the positions p_1 and p_2 to the kth probe, respectively.

$$F\left(d_{p1,k}\right) = \frac{4\pi d_{p1,k}}{\lambda} \tag{34}$$

The power weights of the probes can then be obtained by solving the following objective function

$$\mathbf{G} = \arg\min \sum_{q=1}^{Q} |\rho_q - \hat{\rho}_q|^2 \tag{35}$$

2) Similarity of the power angular spectrum [86]

The PAS can be obtained from the Barlett beamforming algorithm, which calculates the angle by measuring the signal power at each possible AoA and selecting the maximum power direction as the estimate of the AoA. The target PAS estimate can be written as

$$p\left(\Omega\right)=a^{H}\left(\Omega\right)\mathbf{R}a\left(\Omega\right), \tag{36}$$

where $a\left(\Omega\right)$ is the steering vector of the DUT to the spatial angle Ω. $\mathbf{R}$ is the target channel spatial correlation, where the element is ρ_q. For emulated channels in the chamber, the PAS estimate can be written as

$$\hat{p}\left(\Omega\right)=a^{H}\left(\Omega\right)\hat{\mathbf{R}}a\left(\Omega\right), \tag{37}$$

where $\hat{\mathbf{R}}$ is the emulated channel spatial correlation, where the element is $\hat{\rho}_q$. Therefore, the objective function can be written as

$$\min_{\mathbf{G}} \parallel \boldsymbol{p}-\hat{\boldsymbol{p}} \parallel_2^2 \quad \text{s.t.} \parallel \mathbf{G} \parallel=1, 0\leqslant g_k\leqslant 1. \tag{38}$$

According to the obtained OTA antenna power weights, the channel matrix of the emulated channel can be written as [87]

$$\begin{aligned} h_{s,k,n}^{\mathrm{OTA}}\left(f,t\right)=&\sqrt{\frac{P_n}{M}}\sum_{m=1}^{M}f_s^{\mathrm{Tx}}\left(\Omega_{n,m}^{\mathrm{Tx}}\right)\sqrt{g_{n,m,k}}\times\exp\left(\frac{j2\pi\hat{r}_{s,n,m}\cdot\vec{d}_{tx,s}}{\lambda}\right)\\ &\times\exp\left(j2\pi v_{n,m}t+j\Phi_{n,m,k}-j2\pi f\tau_n\right) \end{aligned} \tag{39}$$

$$\hat{h}_{u,s,n}\left(f,t\right)=\sum_{k=1}^{K}f^{\mathrm{OTA}}\left(\Omega_{n,k}^{\mathrm{OTA}}\right)f_u^{\mathrm{Rx}}\left(\Omega_{n,k}^{\mathrm{OTA}}\right)\alpha_{k,u}h_{s,k,n}^{\mathrm{OTA}}\left(f,t\right) \tag{40}$$

where $\Omega_{n,m}^{\mathrm{Tx}}$ is the solid AoD of the mth subpath of the nth cluster; $g_{n,m,k}$ is the power weights of the kth probe of the mth subpath of the nth cluster; K is the number of the active probes; $\hat{r}_{s,n,m}$ is the spherical unit vector corresponding to the angles of departure of the mth subpath of the nth cluster; $\vec{d}_{tx,s}$ is the location vector of transmit antenna element s; denotes the dot product operator; f^{OTA} is the OTA antenna pattern; $\Omega_{n,k}$ is the solid AoA of the kth probe of the nth cluster; $\alpha_{k,u}$ is the propagation coefficient from the kth probe antenna to the uth DUT antenna element.

3.2 Channel emulation accuracy

New metrics are needed to evaluate the performance of millimeter-wave terminals and adaptive antenna systems [28, 88]. PAS-based metrics (i.e. PAS estimation and spatial correlation) are adopted to evaluate 4G antenna systems. For 5G antenna systems, two additional metrics about beam probability are considered.

1) Beam peak distance

Beam peak distance is the angular distance between probability weighted average directions of the allocated beams. It is defined as

$$D_b=\left\|\sum_{b=1}^{B}\Omega_b p_r\left(\Omega_b\right)-\Omega_b p_o\left(\Omega_b\right)\right\|, \tag{41}$$

where Ω_b denotes the spatial angle of the bth beam; $p_r\left(\Omega_b\right)$ and $p_o\left(\Omega_b\right)$ denote the probability of detecting the maximum power in the bth beam for the target and OTA case, respectively [89].

2) Total variation distance of beam allocation distributions

This variation is defined as

$$D_s=\sum_{b}\frac{\left|p_r\left(\Omega_b\right)-p_o\left(\Omega_b\right)\right|}{2}. \tag{42}$$

The range of is $[0, 1]$, where 0 represents complete similarity and 1 represents complete dissimilarity. It has been demonstrated [90] that total variation distance of beam allocation distributions might be more helpful than the beam peak distance for 5G OTA testing.

3) Total variation distance of power angular spectrum

This metric reflects both the PAS itself and the size and resolution of the DUT. It is defined as

$$D_p = \frac{1}{2}\int \left| \frac{\hat{P}_r(\Omega)}{\int \hat{P}_r(\Omega')\, d\Omega'} - \frac{\hat{P}_o(\Omega)}{\int \hat{P}_o(\Omega')\, d\Omega'} \right| d\Omega. \tag{43}$$

Then, the similarity between the target and the simulated beamforming power pattern can be defined as [91]

$$S = (1 - D_p) \times 100\%, \tag{44}$$

where $\hat{P}_r(\Omega)$ and $\hat{P}_o(\Omega)$ are PAS estimates of the reference channel and emulated channel obtained by the Bartlett beamforming method, respectively.

4) spatial correlation

The weighted root mean square (RMS) spatial correlation error is defined as

$$e_\rho = \sqrt{\frac{1}{Q}\sum_{q=1}^{Q} |\rho_q - \hat{\rho}_q|^2 \max(|\rho_q|, |\hat{\rho}_q|)}, \tag{45}$$

where ρ_q and $\hat{\rho}_q$ represent the spatial correlation of position pair $q = (\boldsymbol{p}_{q1}, \boldsymbol{p}_{q2})$ of the target and emulated channel, respectively. Q represents the number of the total position pairs.

3.3 Emulation of dynamic radio channel

It is important to evaluate massive MIMO devices under dynamic channel conditions because of the following reasons [92]:

1) Hybrid beamforming is significant in the millimeter band, which will cause the channel to become highly dynamic.

2) The link distance is short at the millimeter-wave frequency, so even a short distance of the movement can cause a change in the channel spatial structure.

3) Path gain is very sensitive to obstacles, which results in rapid changes in power levels observed by different multipath components.

However, because the channel is dynamic (i.e. time varying), the PAS is also time varying, which requires the selection of the active antenna probes and the weights of the antenna probes to be updated in real time as the channel changes. Considering that the probe weights optimization method in section IV-A is computational in the case of dynamic channels, an efficient and simple computational method has been proposed. This approach is based on minimizing the target PAS and the reconstructed PAS in the OTA case. First, form a steering vector matrix from the DUT array to the OTA probe directions, i.e. $\mathbf{A} = [\mathbf{a}(\Omega_1) ... \mathbf{a}(\Omega_K)] \in \mathbb{C}^{M\times K}$.

Similar to (37), the PAS estimate defined to the K probe directions is defined as

$$\hat{\mathbf{P}}_o = \mathbf{A}^H \mathbf{R} \mathbf{A} \in^{K\times K} . \tag{46}$$

Then the power weight vector can be obtained by

$$\mathbf{W} = \left| \mathrm{diag}\left(\hat{\mathbf{P}}_o\right) \right| \in \mathbb{R}^{K\times 1}, \tag{47}$$

where diag $(\cdot)$ represents getting the diagonal elements in the matrix and puts them into a column vector.

This simple weights calculation method greatly reduces the computational complexity because no numerical optimization is involved in the calculation process. Other study findings [92, 93] have proven the feasibility of this approach.

3.4 Rrequirements of the 3D BS test system design

3.4.1 *Flexible probe selection algorithm*

To save the system cost, a few flexible probe selection algorithms including multishot, artificial bee colony (ABC) and particle swarm optimization (PSO) have been proposed to reduce the number of probes.

1) Multishot algorithm [31, 94]

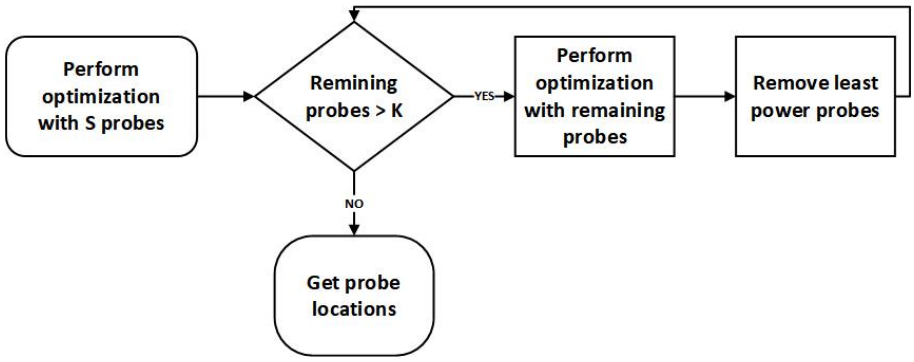

Figure 5 Flowchart of the multishot algorithm.

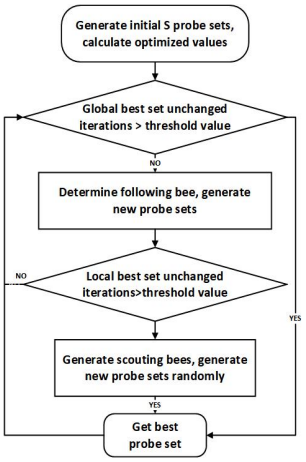

Figure 6 Flowchart of the artificial bee colony algorithm.

The purpose of the multishot algorithm is to remove several probes with the least contribution after each iteration until K probes are retained (Figure 5). Supposing the number of available probes is N.

2) Artificial bee colony algorithm [94]

The ABC algorithm is an optimization method proposed by imitating bee behavior (Figure 6). It only needs to compare the advantages and disadvantages of the problem without understanding the special information of the problem, and the global optimal value would emerge by local optimization behavior of individual artificial bees. The ABC algorithm provides faster convergence speed than the other algorithms. Additionally, it outperforms compared to the multishot algorithm when the number of probes is limited [94].

3) Particle swarm optimization algorithm [75, 95]

The PSO algorithm mimics the clustering behavior of insects, herds and birds (Figure 7). These groups look for food in a collaborative way, and each member of the group continually changes its search model by learning and observing the experience of other members. The core of the PSO algorithm is the speed and position update principle.

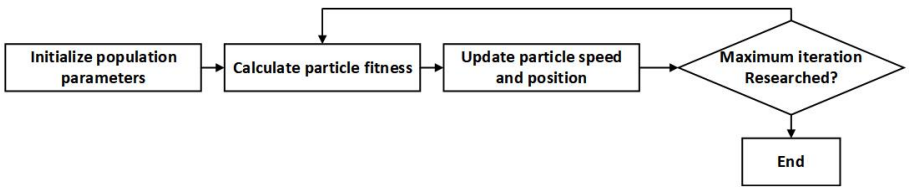

Figure 7 Flowchart of the particle swarm optimization algorithm.

3.4.2 *Size of Testing Setup*

Studies [96, 97] have evaluated the measurement distance of the massive MIMO BS radiated OTA test setup (i.e. the distance R from the probe to the center of the test area). One study [97] focused on the frequency of 28 GHz, whereas another [96] aimed to determine whether traditional far-field criteria must be followed when determining the measurement range. In the link budget analysis, 28 GHz was excluded because the setup and demand for millimeter-wave cellular systems are not yet clear, and the link budget analysis for 2.6 GHz and 3.5 GHz was based on current LTE parameters. For the downlink, the power at the input of the UE emulator can be written in dB as

$$P_E = P_{TX,BS} + G_{TX} - 10\log_{10}\left[\left(\frac{4\pi R f_c}{c}\right)^2\right] + G_P + G_c + G_{CE}, \tag{48}$$

where $P_{TX,BS}$ denotes Tx power of the BS; G_{TX} denotes the BS antenna gain; R is the measurement range; c is the speed of light; f_c is the center frequency; G_P is the probe antenna gain; G_c is the OTA cable loss and G_{CE} is the channel emulator gain.

The power at the BS input can be similarly written according to equation (48) for uplink transmission. Because the transmit power of UE is much smaller than that of the BS, the UE has stricter requirements on the power link budget. For the uplink, the -90dBm Energy Per Resource Element is used as the target. Therefore, it is concluded that the maximum R of 2.6GHz is 5m, and the maximum R of 3.5GHz is 3.5m. Of course, the link budget analysis used here is only an approximation, because only one BS and one probe are considered in the analysis. Thus, the possible array gain is not considered.

Field performance analysis (e.g. amplitude error, angular error and phase error) at different frequencies (e.g. 2.6 GHz, 3.5 GHz and 28 GHz) indicates that the demand for R decreases as the frequency increases. In the DoA simulation accuracy analysis, the beamforming algorithm, which is insensitive to error, is used to verify that the DoA can be well estimated even if the far-field distance is not satisfied.

Multi-user MIMO (MU-MIMO) sum rate capacity is another important metric for evaluating OTA setup measurement distance for high and low frequencies. For the high frequency such as 28 GHz, the MU-MIMO sum rate capacity is presupposed to be full degrees of freedom in combining elements of the BS array. Several of the UEs can be randomly selected as a sub-set for each simulation, and the simulation can be repeated for many (e.g. hundreds) random UE sub-sets. By a sub-optimal linear pre-coding method (forcing zero), the linear pre-coding vectors can be determined for each UE

$$\mathbf{W}(t) = \mathbf{H}^H(t)\left(\mathbf{H}(t)\,\mathbf{H}^H(t)\right)^{-1}, \tag{49}$$

where $\mathbf{H}(t)$ is the composite channel transmission matrix for one UE sub-set and all BS elements. $\mathbf{w}_k(t)$ represents the kth row of $\mathbf{W}(t)$ and it is normalized. Then, the sum rate capacity can be calculated as

$$C(t) = \sum_{k=1}^{K} 1\log_2\left(1 + \frac{\gamma}{K}\left|\mathbf{w}_k(t)\,\mathbf{h}_k(t)\right|^2\right), \tag{50}$$

where γ is the signal to noise ratio and $\mathbf{h}_k(t)$ is the kth column vector of $\mathbf{H}(t)$. The simulation results show that even if the measurement distance R is smaller than the far-field criteria, the error of MU-MIMO sum rate capacity is not obvious compared to the far field (R=1000m).

Another important metric called fixed beam power loss for the 28 GHz evaluation has been proposed [97]. It is necessary to assume that the communication system has fixed beams, that is, with a discrete code book of BS antenna weights. The BS array can at least partially use analog beamforming to compose beams into a pre-defined set of directions. The loss in the kth probe direction can be expressed as

$$Q_k = \left|\frac{1}{M}\sum_{m=1}^{M}\cos\left(\beta_{k,m} - \alpha_{k,m}\right)\right|^2. \tag{51}$$

where $\alpha_{k,m}$ is the spherical wave phase error from the kth probe to the mth DUT element with respect to the phase in the origin.

$$\alpha_{k,m} = \frac{2\pi}{\lambda}\left(\|\vec{a}_k - \vec{b}_m\| - R\right), \tag{52}$$

where $\vec{a}_k$ represents the position vector of the kth probe; $\vec{b}_m$ represents the position vector of the mth DUT element. $\beta_{k,m}$ is the phase error of the kth probe direction for a planar wavefront and can be calculated as

$$\beta_{k,m} = \frac{-\vec{a}_k}{\|\vec{a}_k\|} \cdot \vec{b}_m \frac{2\pi}{\lambda}. \tag{53}$$

Then, the average fixed beam power loss of the K probe locations can be calculated as

$$Q_{av} = \frac{1}{K} \sum_{k=1}^{K} Q_k. \tag{54}$$

If the acceptable error threshold is assumed to be 2 dB, then the relationship between the maximum dimension D and measurement R can be approximated as a linear function $R = 14.46D - 1.1$. If the BS is assumed to be a 20×20 planar array and the element spacing is 0.5λ, then the minimum value of R can be approximated to be 0.85m [97].

It can be seen from the above analysis that for the massive MIMO BS OTA testing, the measurement distance R does not necessarily have to meet the far-field criteria, and the far-field requirement can be appropriately relieved [96].

4 New testing methods for 5G radios

4.1 Fifth generation massive virtual testing

The installation of the practical anechoic chamber, the probe plane and the implementation of the switching circuit can be complex and costly for the 3D sectored MPAC OTA test setup. Thus, a virtual OTA testing method has been proposed, and the concept of the flexible virtual probe has been adopted. The main idea of this method is to replace the anechoic chamber, probe plane and switching circuit with a phase matrix [98]. The probe selection method is the same as that proposed in section 5.1, and the phase matrix can be written as

$$\mathbf{F} = \{f_{m,k} = e^{j\frac{2\pi}{\lambda}\vec{r}_m \cdot \vec{\hat{\Omega}}_k}\}, \tag{55}$$

where $\vec{r}_m$ is the unit vector of the mth DUT element and $\vec{\hat{\Omega}}_k$ is the unit position vector of solid angle of the kth probe.

The feasibility of this method has been verified by three metrics, including spatial correlation error, total variation distance of PAS and beam statistic distance [98].

4.2 New method based on reflective properties of concave surfaces

Obviously, 3D sectored MPAC setup is not suitable for the UE in which full 3D is preferred. The proposed method can generate highly dynamic 3D environments by making use of reflective properties of concave surfaces (ellipsoid and elliptical cylinder reflectors) to emulate real-life millimeter-wave frequencies channel propagation scenarios.

The test setup comprises an ellipsoid of revolution or a set of elliptical cylinder reflectors, a feeder antenna, a DUT and a BS emulator. The feeder antenna should be an array antenna which can generate multiple simultaneous independent beams. The DUT and feeder antenna are placed at focal points, respectively. The ray emanated from one focal point would arrive at another focal point. Initial test results have been described [99], implemented with an elliptical cylinder reflector.

In addition, the concept of a single-probe measurement system has been proposed [100] for 5G 3D channel emulation while reducing system costs.

5 Conclusion

This review discussed technical points of MIMO OTA testing in the anechoic chamber setup. The channel emulation methods, including PFS, PWS, and EIV methods in 2D UE MIMO OTA testing and PFS method in 3D BS MIMO OTA testing are presented. Some key aspects of MPAC setup are also studied, such as test zone size, physical dimension of the setup and number of probes and so on. Two

measurement setups are introduced in this paper: a 2D uniform MPAC and a 3D sectored MPAC. The 3D sectored MPAC setup is proposed to accurately reproduce the desired propagation channels, while the cost of the setup can be significantly reduced in the massive BS antennas OTA testing. The setup is cost-effective mainly because the corresponding hardware resources are reduced, for example, the active probes required are reduced by switching circuits, and the DUT is placed on the one side of the anechoic chamber to reduce the chamber size, etc. Some novel massive test methods are also included in this paper. Future research should focus on new techniques and algorithms to save costs related to MPAC setups. In addition, the active probes selection algorithm with lower computational complexity, the definition of the mmWave channel emulation metrics error threshold, and the calibration of the mmWave test system are all required further research. For the novel massive test methods, there are some follow-up research work such as the practical realization of the programming phase matrix of the virtual OTA test system and so on.

Acknowledgements This work was supported in part by National Natural Science Foundation of China under grants 61801366, 81701774, and 61771423, Natural Science Foundation of Shaanxi Province under Grant 2020JM-078, National Key Research and Development Program of China (2018YFA0701400), Zhejiang Lab (2018EB0ZX01), Key-Area Research and Development Program of Guangdong Province (2018B030333001), and the Fundamental Research Funds for the Central Universities (2019XZZX003-20).

References

1 3GPP TS 34.114, User equipment (UE) / mobile station (MS) over the air (OTA) antenna performance; conformance testing (release 7). 2009
2 CTIA Certifification, Test Plan for Mobile Station Over the Air Performance, Method of Measurement for Radiated RF Power and Receiver Performance, Revision Number 2.2.2, 2008
3 Obayashi S, Ohishi T, Karasawa Y. Effect of vertical angle spread of propagation channel on MIMO OTA measurement method. In: Proceedings of 2010 Asia-Pacific Microwave Conference, Yokohama, 2010. 1934-1937
4 Rumney M, Pirkl R, Landmann M, et al. MIMO over-the-air research, development, and testing. International Journal of Antennas and Propagation, 2012, 2012: 1-8
5 Jing Y, Zhao X, Kong H W, et al. Two stage over-the-air (OTA) test method for LTE MIMO device performance evaluation. International Journal of Antennas and Propagation, 2012, 2012: 1-6
6 Kyösti P, Jämsö T, Nuutinen J-P. Channel modelling for multiprobe over-the-air MIMO testing. International Journal of Antennas and Propagation, 2012, 2012: 1-11
7 Arsalane N, Mouhamadou M, Decroze C, et al. 3GPP channel model emulation with analysis of MIMO LTE performances in reverberation chamber. International Journal of Antennas and Propagation, 2012, 2012: 1-8
8 Kildal P S, Rosengren K. Correlation and capacity of MIMO systems and mutual coupling, radiation effificiency, and diversity gain of their antennas: Simulations and measurements in a reverberation chamber. IEEE Communications Magazine, 2004, 42: 104-112
9 Chen X M. Throughput modeling and measurement in an isotropic scattering reverberation chamber. IEEE Transactions on Antennas and Propagation, 2014, 62: 2130-2139
10 Yu W, Qi Y H, Liu K F, et al. Radiated two-stage method for LTE MIMO user equipment performance evaluation. IEEE Transactions on Electromagnetic Compatibility, 2014, 56: 1691-1696
11 Fan W, Kyösti P, Hentilä, et al. MIMO terminal performance evaluation with a novel wireless cable method. IEEE Transactions on Antennas and Propagation, 2017, 65: 4803-4814
12 Toivanen J T, Laitinen T A, Kolmonen V M, et al. Reproduction of arbitrary multipath environments in laboratory conditions. IEEE Transactions on Instrumentation and Measurement, 2011, 60: 275-281
13 Sharma R K, Kotterman W, Landmann M H, et al. Over-the-air testing of cognitive radio nodes in a virtual electromagnetic environment. International Journal of Antennas and Propagation, 2013, 2013: 1-16
14 Khatun A, Kolmonen V M, Hovinen V, et al. Experimental verifification of a plane-wave field synthesis technique for MIMO OTA antenna testing. IEEE Transactions on Antennas and Propagation, 2016, 64: 3141-3150
15 Llorente I C, Fan W, Nielsen J ∅, et al. Comparison of channel emulation techniques in multiprobe anechoic chamber setups. In: Proceedings of the 9th European Conference on Antennas and Propagation (EuCAP), Lisbon, 2015. 1-5
16 Fan W, Carreño X, Kyösti P, et al. Over-the-air testing of MIMO-capable terminals: evaluation of multiple-antenna systems in realistic multipath propagation environments using an OTA method. IEEE Vehicular Technology Magazine, 2015, 10: 38-46
17 Mow M A, Niu B L, Schlub R W, et al. Tools for design and analysis of over-the-air test systems with channel model emulation capabilities. U.S. Patent 20 110 270 567, 2011
18 Kyösti P, Nuutinen J. Over the air test. U.S. Patent 20 110 189962, 2011
19 Reed J D. Emulation and controlled testing of MIMO OTA channels. U.S. Patent 20 110 299 570, 2011
20 Erceg V, Schumacher L, Kyritsi P, et al. TGn channel models, IEEE P802.11 wireless LANs, http://www.802wirelessworld.com:8802/. Tech. Rep., IEEE, 2004
21 Baum D S, Hansen J, Salo J, et al. An interim channel model for beyond-3G systems: extending the 3GPP spatial channel model (SCM). In: Proceedings of IEEE 61st Vehicular Technology Conference, Stockholm, 2005. 3132-3136
22 Kyösti P, Meinilö J, Hentilö L, et al. ST-4-027756 WINNER II deliverable 1.1.2. v.1.2, WINNER II channel models. Tech. Rep. IST-WINNER2, 2007
23 Study on cannel model for frequencies from 0.5 to 100 GHz, Version TR 38.901, document TR 38.901 3GPP, July 2017
24 Wu X F, Wang N, Zhang Z H, et al. Comparison tests and hand phantom standardization for multi-probe based MIMO OTA. In: Proceedings of IEEE 5th Asia-Pacific Conference on Antennas and Propagation (APCAP), Taiwan, 2016. 321-322
25 Fan W, Kyösti P, Hentilä L, et al. Experimental evaluation of MIMO terminals with user influence in OTA setups. IEEE Antennas and Wireless Propagation Letters, 2017, 16: 3030-3033
26 Carreño X, Fan W, Nielsen J ∅, et al. Test setup for anechoic room based MIMO OTA testing of LTE terminals. In: Proceedings of the 7th European Conference on Antennas and Propagation (EuCAP), Gothenburg, 2013. 1417-1420

27 Test plan for 2×2 Downlink MIMO and transmit diversity over-the air performance. CTIA Certifiification, Tech. Rep., Version 1.1, 2016

28 Kyösti P, Hentilä L, Fan W, et al. On radiated performance evaluation of massive MIMO devices in muilti-probe anechoic chamber OTA setups. IEEE Transactions on Antennas and Propagation, 2018, 66: 5485-5497

29 Wang W M, Li M Y, Liu Y A, et al. Novel physical probe configurations in a multi-probe based 3D MIMO OTA setup. The Journal of China Universities of Posts and Telecommunications, 2017, 24: 60-66

30 Wang R R, Wang W M, Wu Y G, et al. 3D channel spatial characteristic emulation in multi-probe anechoic chamber setups. In: Proceedings of Global Wireless Summit (GWS), Chiang Rai, 2018. 348-353

31 Yuan Y, Wang W M, Liu Y N, et al. Impact of probe ring location on test area performance in 3D MIMO OTA setup. In: Proceedings of the 11th International Symposium on Antennas, Propagation and EM Theory (ISAPE), Guilin, 2016. 858-861

32 Zhang Z, Tian L, Zhang J H, et al. Analysis of test volume size in 3D MIMO OTA for 5G. In: Proceedings of IEEE International Conference on Communications Workshops (ICC Workshops), Shanghai, 2019. 1-6

33 Fan W, Sun F, Nielsen J ∅, et al. Probe selection in multiprobe OTA setups. IEEE Transactions on Antennas and Propagation, 2014, 62: 2109-2120.

34 Yang X L, Zhang P, Chen J Q, et al. Probe subset selection in 3D multiprobe OTA setup. In: Proceedings of IEEE 29th Annual International Symposium on Personal, Indoor and Mobile Radio Communications (PIMRC), Bologna, 2018. 1-6

35 Fan W, Szini I, Nielsen J ∅, et al. Channel spatial correlation reconstruction in flexible multiprobe setups. IEEE Antennas and Wireless Propagation Letters, 2013, 12: 1724-1727

36 Gao H Q, Wang W M, Wu Y L, et al. 3D flexible multi-probe setups for MIMO OTA testing. In: Proceedings of the 5th International Symposium on Electromagnetic Compatibility, Beijing, 2017. 1-4

37 Wang W M, Wang R R, Gao H Q, et al. Implementation and analysis of 3D channel emulation method in multi-probe anechoic chamber setups. IEEE Access, 2019, 7: 108571-108580

38 Jungnickel V, Jaeckel S, Thiele L, et al. Capacity measurements in a cooperative MIMO network. IEEE Transactions on Vehicular Technology, 2009, 58: 2392?2405

39 Fan W, Kyösti P, Nielsen J ∅, et al. Wideband MIMO channel capacity analysis in multiprobe anechoic chamber setups. IEEE Transactions on Vehicular Technology, 2016, 65: 2861-2871

40 Fan W, Kyösti P, Nuutinen J-P, et al. On probe weighting for MIMO OTA testing in anechoic chamber setups. In: Proceedings of Asia-Pacific Microwave Conference (APMC), Nanjing, 2015. 1-3

41 Belhabib M, D'Errico R, Bernard U. Effect of finite ring radius and antenna radiation on spatial correlation in multiprobe Over-The-Air tests. In: Proceedings of the 10th European Conference on Antennas and Propagation (EuCAP), Davos, 2016. 1-5

42 Belhabib M, D'Errico R, Uguen B. Spatial correlation in spherical and cylindrical 3D MIMO over-the-air tests setups. In: Proceedings of the 10th European Conference on Antennas and Propagation (EuCAP), Davos, 2016. 1-4

43 Fan W, Szini I, Foegelle M D, et al. Measurement uncertainty investigation in the multi-probe OTA setups. In: Proceedings of the 8th European Conference on Antennas and Propagation (EuCAP), Hague, 2014. 1068-1072

44 Fan W, Carreño X, Nielsen J ∅, et al. Measurement verification of plane wave synthesis technique based on multi-probe MIMO-OTA setup. In: Proceedings of IEEE Vehicular Technology Conference (VTC Fall), Quebec City, 2012. 1-5

45 Foged L J, Scannavini A, Gross N, et al. MIMO OTA testing using a multiprobe system approach. In: Proceedings of the 7th European Conference on Antennas and Propagation (EuCAP), Gothenburg, 2013. 1673-1677

46 Guo L, Sun C, An X D, et al. Over the air MIMO channel model validation. In: Proceedings of the 7th European Conference on Antennas and Propagation (EuCAP), Gothenburg, 2013. 1848-1852

47 Fan W, Nielsen J ∅, Carreño X, et al. Impact of system non-idealities on spatial correlation emulation in a multi-probe based MIMO OTA setup. In: Proceedings of the 7th European Conference on Antennas and Propagation (EuCAP), Gothenburg, 2013. 1663-1667

48 Fan W, Nielsen J ∅, Carreño X, et al. Impact of probe placement error on MIMO OTA test zone performance. In: Proceedings of Loughborough Antennas and Propagation Conference (LAPC), Loughborough, 2012. 1-4

49 Reed D. Experiments with spatial correlation for evaluating OTA techniques TD (09)856. COST2100, 2009. 1-4

50 Fan W, Carreño X, Lisbone B d, et al. Emulating spatial characteristics of MIMO channels for OTA testing. IEEE Transactions on Antennas and Propagation, 2013, 61: 4306-4314

51 Boyd S, Vandenberghe L. Convex optimization. Cambridge, U.K.: Cambridge Univ. Press, 2004

52 Llorente I C, Fan W, Pedersen G F. MIMO OTA esting in small multiprobe anechoic chamber setups. IEEE Antennas and Wireless Propagation Letters, 2015, 15: 1167-1170

53 Parveg D, Laitinen T, Khatun A, et al. Calibration procedure for 2-D MIMO over-the-air multi-probe test system. In: Proceedings of the 6th European Conference on Antennas and Propagation (EUCAP), Prague, 2012. 1594-1598

54 Fan W, Nielsen J ∅, Franek O, et al. Antenna pattern impact on MIMO OTA testing. IEEE Transactions on Antennas and Propagation, 2013, 61: 5714-5723

55 Kotterman W A T, Heuberger A, Thomä R S. On the accuracy of synthesised wave-fields in MIMO-OTA setups. In: Proceedings of the 5th European Conference on Antennas and Propagation (EUCAP), Rome, 2011. 2560-2564

56 Laitinen T A, Kyösti P, Nuutinen J-P, et al. On the number of OTA antenna elements for plane-wave synthesis in a MIMO OTA test system involving a circular antenna array. In: Proceedings of the 4th European Conference on Antennas and Propagation (EUCAP), Barcelona, 2010. 1-5

57 Schirmer C, Landmann M H, Kotterman W A T, et al. 3D wave-field synthesis for testing of radio devices. In: Proceedings of the 8th European Conference on Antennas and Propagation (EuCAP), Hague, 2014. 3394-3398

58 Fan W, Kyösti P, Hentilä L, et al. Rician channel modeling for multiprobe anechoic chamber setups. IEEE Antennas and Wireless Propagation Letters, 2014, 13: 1761-1764

59 Ji Y L, Fan W, Pedersen G F, et al. On channel emulation methods in multi-probe anechoic chamber setups for over-the-air testing. IEEE Transactions on Vehicular Technology, 2018, 67: 6740-6751

60 Giacaglia G. Trigonometric interpolation. Celestial Mechanics, 1970, 1: 360-367

61 Kyösti P, Khatun A. Probe configurations for 3-D MIMO over-the-air testing. In: Proceedings of the 7th European Conference on Antennas and Propagation (EuCAP), Gothenburg, 2013. 1421-1425

62 Fan W, Sun F, Kyösti P, et al. 3D channel emulation in multi-probe setup. Electronics Letters, 2013, 49: 623-625

63 Fan W, Hentilä L, Kyösti P, et al. Test zone size characterization with measured MIMO throughput for simulated MPAC configurations in conductive setups. IEEE Transactions on Vehicular Technology, 2017, 66: 10532-10536

64 Laitinen T, Toivanen J, Kyösti P, et al. On a MIMO-OTA testing based on multi-probe technology. In: Proceedings of 2010

URSI International Symposium on Electromagnetic Theory, Berlin, 2010. 227-230
65 Kyösti P, Nuutinen J, Jämsä T. Simulated correlation accuracy of MIMO OTA spatial fading emulator. In: Proceedings of COST-2100, 11th MCM, Alborg, 2010
66 Imai T, Okano Y, Koshiro K, et al. Theoretical analysis of adequate number of probe antennas in spatial channel emulator for mimo performance evaluation of mobile terminals. In: Proceedings of the 4th European Conference on Antennas and Propagation (EuCAP), Barcelona, 2010. 1-5
67 Panasonic and Tokyo Institute of Technology. Procedure of the determining the dimension of a spatial fading emulator. In: Proceedings of 3GPP TSG RAN4 Meeting, Jeju, 2009
68 Laitinen T, Kyösti P, Jämsä T, et al. Generation of a field with a laplacian-distributed power azimuth spectrum scattered by a single cluster in a MIMO-OTA test system based on multiple probe antennas. In: Proceedings of Asia-Pacific Microwave Conference, Yokohama, 2010. 2127-2130
69 Khatun A, Laitinen T, Kolmonen V-M, et al. Dependence of error level on the number of probes in over-the-air multiprobe test systems. International Journal of Antennas and Propagation, 2012, 2012: 1-6
70 Khatun A, Kolmonen V-M, Laitinen T, et al. Clarification of uncertainties in MIMO over-the-air multi-probe test systems. In: Proceedings of the 7th European Conference on Antennas and Propagation (EuCAP), Gothenburg, 2013. 1427-1431
71 Scannavini A, FogedL J, Gross N, et al. Test zone characterization for the multiprobe anechoic chamber setup (MPAC). In: Proceedings of the 10th European Conference on Antennas and Propagation (EuCAP), Davos, 2016. 1-5
72 Fan W, Kyösti P, Ji Y L, et al. Experimental evaluation of user influence on test zone size in multi-probe anechoic chamber setups. IEEE Access, 2017, 5: 18545-18556
73 Yamamoto A. Procedure of designing the structural parameters of a spatial fading emulator with a Laplacian angular power spectrum of incoming wave. In: Proceedings of COST 2100 TD(10)10016, Athens, 2010.
74 Kyösti P, Hentilä L. Criteria for physical dimensions of MIMO OTA multi-probe test setup. In: Proceedings of the 6th European Conference on Antennas and Propagation (EUCAP), Prague, 2012. 2055-2059
75 Wang W M, Wang H, Gao H Q, et al. Plane wave compensation technique for MIMO OTA testing in small multi-probe anechoic chamber. IET Microwaves Antennas and Propagation, 2019, 13(9)
76 Fan W, Pedersen G F, Kyösti P, et al. Recent advances on OTA testing for 5G antenna systems in multi-probe anechoic chamber setups. In: Proceedings of the 6th Asia-Pacific Conference on Antennas and Propagation (APCAP), Xi'an, 2017. 1-3
77 Reed D, Borsato R, Rodriguez-Herrera A. Evaluation of devices with adaptive antennas using over the air techniques. In: Proceedings of the 10th European Conference on Antennas and Propagation (EUCAP), Davos, 2016. 1-5
78 Fan W, Kyösti P, Rumney M, et al. Over-the-air radiated testing of millimeter-wave beam-steerable devices in a cost-Effective measurement setup. IEEE Communications Magazine, 2018, 56: 64-71.
79 Fan W, Zhang F C, Jämsä T, et al. Reproducing standard SCME channel models for massive MIMO base station radiated testing. In: Proceedings of the 11th European Conference on Antennas and Propagation (EUCAP), Paris, 2017: 3658-3662
80 Fan W, Carton I, Kyösti P, et al. A step toward 5G in 2020: low-cost OTA performance evaluation of massive MIMO base stations. IEEE Antennas and Propagation Magazine, 2017, 59: 38-47
81 Fan W, Zhang F C, Wang Z P, et al. Validation of test environment in simple sectored MPAC setups for over-the-air testing of 5G communication systems. IEEE Antennas and Propagation Magazine, 2019. doi: 10.1109/MAP.2019.2943305.
82 Kotterman W A T, Schirmer C, Landmann M H, et al. New challenges in over-the-air testing. In: Proceedings of the 11th European Conference on Antennas and Propagation (EUCAP), Paris, 2017. 3676-3678
83 Khatun A, Haneda K, Heino M, et al. Feasibility of multi-probe over-the-air antenna test methods for frequencies above 6 GHz. In: Proceedings of 2015 Loughborough Antennas and Propagation Conference (LAPC), Loughborough, 2015. 1-5
84 Wang H, Wang W M, Wu Y, et al. Probe selection for 5G massive MIMO base station over-the-air testing. IEEE Antennas and Wireless Propagation Letters, 2020, 19: 1998-2002
85 Qiao Z L, Xie Y J, Wang Z P, et al. Exploring OTA testing for massive MIMO base stations in small region. In: Proceedings of the 6th Asia-Pacific Conference on Antennas and Propagation (APCAP), Xi'an, 2017. 1-3
86 Ji Y L, Xin L J, Zhang X. On probe weighting for massive MIMO OTA testing based on angular spectrum similarity. IEEE Antennas and Wireless Propagation Letters, 2019, 18: 1497-1501
87 Pei H L, Chen X M, Fan W, et al. Comparisons of channel emulation methods for state-of-the-art multi-probe anechoic chamber based millimeter-wave over-the-air testing. In: Proceedings of 2019 IEEE 90th Vehicular Technology Conference (VTC2019-Fall), Honolulu, 2019. 1-5
88 Hekkala A, Kyösti P, Kyröläinen J, et al. Performance evaluation of sectored MPAC for 5G UE antenna systems. In: Proceedings of the 6th Asia-Pacific Conference on Antennas and Propagation (APCAP), Xi'an, 2017. 1-3
89 Gao H Q, Wang W M, Fan W, et al. Beam probability metric for 5G OTA testing in multi-probe anechoic chamber setups. In: Proceedings of 2019 IEEE International Symposium on Antennas and Propagation and USNC-URSI Radio Science Meeting, Atlanta, 2019. 1847-1848
90 Gao H Q, Wang W M, Fan W, et al. Beam probability metric for OTA testing of adaptive antenna systems in multi-probe anechoic chamber setups. In: Proceedings of the 13th European Conference on Antennas and Propagation (EuCAP), Krakow, 2019. 1-5
91 Zhang F C, Fan W, Ji Y L, et al. Performance testing of massive MIMO base station with multi-probe anechoic chamber setups. In: Proceedings of the 12th European Conference on Antennas and Propagation (EuCAP), London, 2018. 1-5
92 Zhang X, Qiao S B, Peng M G, et al. Probe selection for over-the-air test in 5G base stations with massive multiple-input multiple-output. China Communications, 2019, 16: 1-12
93 Wang H, Wang C Q, Wang W M, et al. Flexible OTA probe setups for massive MIMO base station testing. In: Proceedings of 2018 Asia-Pacific Microwave Conference (APMC), Kyoto, 2018. 908-910
94 Pei H L, Chen X M, Zhang M, et al. Over-the-air testing of 5G millimeter-wave system with adaptive beamforming. In: Proceedings of 2019 IEEE MTT-S International Wireless Symposium (IWS), Guangzhou, 2019. 1-3
95 Gao H Q, Wang W M, Wu Y L, et al. A virtual over-the-air method for 5G massive MIMO base station testing with flexible virtual probes. IEEE Access, 2019, 7: 108474-108485
96 Reyes D, Beach M, Mellios E, et al. Over-the-air test method for 5G mmWave devices with beamforming capabilities. In: Proceedings of 2018 IEEE Globecom Workshops (GC Wkshps), Abu Dhabi, 2018. 1-6
97 Zhang Q W, Loh T H, Zhang W X, et al. Proof of concept experiment for single probe MIMO OTA measurement system. In: Proceedings of the 13th European Conference on Antennas and Propagation (EuCAP), Krakow, 2019. 1-5
98 Kyösti P, Fan W, Pedersen G F, et al. On dimensions of OTA setups for massive MIMO base stations radiated testing. IEEE

Access, 2016, 4: 5971-5981
99 Kyösti P, Fan W, Kyröläinen J. Assessing measurement distances for OTA testing of massive MIMO base station at 28 GHz. In: Proceedings of the 11th European Conference on Antennas and Propagation (EUCAP), Paris, 2017. 3679-3683
100 Kyösti P, Hentilä L, Kyröläinen J, et al. Emulating dynamic radio channels for radiated testing of massive MIMO devices. In: Proceedings of the 12th European Conference on Antennas and Propagation (EuCAP), London, 2018. 1-5